Environmental Science Processes & Impacts

ROYAL SOCIETY OF CHEMISTRY

PAPER

View Article Online
View Journal | View Issue

Cite this: *Environ. Sci.: Processes Impacts*, 2026, **28**, 1015

Wavelength-specific UV LED and far-UVC degradation of microplastics

Thusitha Rathnayake, Paul Onkundi Nyangaresi and Sara E. Beck *

Received 7th October 2025
Accepted 25th February 2026

DOI: 10.1039/d5em00818b

rsc.li/espi

The widespread use and durability of plastics have led to significant global environmental challenges, with microplastics (MPs) recognized as contaminants of emerging concern due to their persistence, accumulation, and potential threats to human health. Photodegradation from ultraviolet (UV) radiation is a critical factor in modifying the physicochemical properties of microplastics through polymer chain scission and the incorporation of oxygen-containing functional groups. These changes can be quantitatively assessed using Fourier transform infrared (FTIR) spectroscopy through the carbonyl index and hydroxyl index. This study addressed the limited understanding of how irradiation from specific UV light-emitting diode (LED) and far-UVC wavelengths distinctly influence the degradation pathways of major polymers, including polyethylene terephthalate (PET), polypropylene (PP), and polyethylene (PE), within environmentally relevant size ranges (300–500 μm). Three additive-free microplastic polymers (PET, PP and PE) were exposed to six discrete UV LED (252, 268, 278, 290, 300, 363 nm) and far-UVC (222 nm) wavelengths, across increasing doses (500–10 000 mJ cm^{-2}). The results demonstrated that UV-induced photo-oxidation of PET, PP, and PE is strongly wavelength-selective, polymer-specific, and frequently non-linear with UV dose. Carbonyl and hydroxyl indices provide complementary, non-interchangeable views of oxidation, while their relationship is polymer-dependent. These results provide quantitative inputs for environmental fate modeling and treatment-relevant weathering assessments of microplastics.

Environmental significance

Microplastic pollution represents a critical environmental challenge due to their prevalence and persistence in aquatic systems. As UV technologies are commonly used in water, wastewater and surface treatment processes, and offer precise wavelength-selectivity, particularly with the emergence of UV light emitting diodes and far-UVC sources, it is critical to understand how individual wavelengths may degrade microplastic polymers. This research demonstrates that photodegradation is strongly wavelength-selective and polymer-specific rather than following universal patterns. By quantifying discrete wavelength and UV-dose effects, these findings enable understanding of microplastics weathering in natural and human made environments and inform development of mechanistic fate models, which directly supports improved environmental risk assessments, optimization of UV treatment applications, and targeted strategies for microplastic pollution control.

1. Introduction

Plastics have revolutionized everyday life due to their affordability, durability, and versatility, yet their enormous production and pervasive use have resulted in significant global environmental challenges. Since plastics are typically derived from fossil fuel hydrocarbons and engineered to resist degradation, they accumulate in both terrestrial and aquatic environments. This persistence results in significant long-term ecological impacts.[1] Recent analysis shows that in 2022, global plastic production reached 400 million metric tons, generating around 267.7 million metric tons of plastic waste, with the recycling rate remaining as low as 9%.[2]

Microplastics, defined as plastic particles smaller than 5 mm, originate from both primary sources, which are deliberately manufactured for industrial or consumer use, and secondary sources, which are formed by the breakdown of larger plastics.[3,4] Microplastics are now recognized as contaminants of emerging concern, capable of being transported through air, water, and soil, and readily entering various ecological compartments and food webs.[5,6] Their primary sources include consumer product usage and disposal, wastewater effluents, stormwater runoff, and atmospheric deposition.[7,8] Once in the environment, microplastics can be ingested by organisms at various trophic levels and transferred through the food chain, leading to adverse biological effects. These include physiological disruptions in exposed organisms and pose potential threats to human health through contaminated food and water supplies.[9,10] Moreover, microplastics serve as

Department of Civil Engineering, University of British Columbia, Vancouver, BC, V6T 1Z4, Canada. E-mail: sara.beck@ubc.ca

vectors for hazardous chemicals, including additives and adsorbed pollutants, such as heavy metals and persistent organic compounds, thus compounding their environmental and health risks.[11,12] Microplastic pollution presents a multifaceted environmental challenge driven by the diversity of polymer types, particle sizes, and their interactions with a variety of environmental factors.

A fundamental factor explaining the persistence and hazards associated with microplastics is their limited degradation potential under natural environmental conditions. Plastics are manufactured with stabilizers, plasticizers, and antioxidants that slow down their breakdown. Over time, both biotic (*i.e.*, biodegradation, bio-disintegration) and abiotic factors contribute to aging of these materials.[11,13] Among these factors, photodegradation induced by ultraviolet (UV) radiation plays a critical role in abiotic degradation, causing polymer chain scission, cross-linking, and the incorporation of oxygen-containing functional groups such as carbonyls and hydroxyls. These chemical modifications result in significant changes to the physicochemical properties of microplastics, including increased polarity, hydrophilicity, surface area, and reactivity. Such changes affect interactions with environmental contaminants.[14–16] UV-induced photodegradation also accelerates fragmentation, increasing the abundance of smaller, more biologically accessible particles, potentially augmenting bioavailability, which is the accessibility and uptake of microplastic particles and their associated chemicals by organisms.[17]

UV LEDs are increasingly being used for water and wastewater treatment and air and surface disinfection given their precise wavelength selectivity, low power consumption, robust operation and longer lifespans in the absence of hazardous materials like mercury.[18] Similarly, far-UVC irradiation is of interest for pandemic mitigation as well as water and wastewater treatment, given its ability to damage proteins as well as nucleic acids, which can inactivate microorganisms without photoreactivation.[18–21] Despite these increased applications, understanding remains limited regarding how irradiation from specific UV LED wavelengths and far-UVC irradiation would distinctly influence degradation pathways of major polymers within environmentally relevant size ranges, particularly 300–500 μm. The detailed transformations of functional groups that characterize microplastic aging under controlled UV exposure are also not completely understood. Investigating how functional group development correlates with UV exposure conditions across specific polymer types and particle sizes is essential to form a comprehensive understanding of microplastic photodegradation. Previous studies have focused narrowly on single wavelengths. For example, studies with UV-C at 254 nm demonstrated the formation of microplastic particles and changes in chemical structures,[22] whereas a recent study with UV-A LEDs at 365 nm revealed morphological changes (*e.g.* surface cracks and pits) as well as the formation of oxygen-containing functional groups.[23]

Our study took advantage of the precise wavelength selectivity of UV LEDs, to investigate the wavelength-dependent effects, of six discrete UV LED wavelengths (252, 268, 278, 290, 300, 363 nm) as well as the far-UVC wavelength of 222 nm at increasing doses on the degradation of microplastics within the 300–500 μm size range. Polyethylene terephthalate (PET), polypropylene (PP), and polyethylene (PE) polymers were chosen because of their widespread use and distinct chemical and physical properties, which make them representative of common environmental microplastics. FTIR is commonly applied for the identification and characterization of microplastics and is particularly useful in detecting chemical alterations associated with weathering. The technique enables the identification of characteristic functional groups and provides a means to track degradation by quantifying indices such as the carbonyl and hydroxyl indices, which increase as photo-oxidation progresses in plastic polymers.[14,24,25] FTIR spectroscopy was employed to quantify functional group evolution in microplastics. To the best of our knowledge, this is the first study to comprehensively examine the effects of far-UVC and UV LED wavelengths in the UV-A, UV-B, and UV-C ranges in degrading environmentally relevant microplastics. The outcomes of this work will enhance the mechanistic understanding of photo-induced chemical transformations in microplastics, providing critical data for improving models of microplastics' environmental fate, persistence, and risks in both freshwater ecosystems and engineered water systems.[16,26]

2. Materials and methods

Microplastic samples of polyethylene terephthalate (PET), polypropylene (PP), and polyethylene (PE) suspended in water were exposed to UV irradiation at weighted average wavelengths of 222, 252, 268, 280, 290, 300, and 363 nm (UV-C to UV-A range) at UV doses of 500, 1000, 1500, 2000, 2500, and 10 000 mJ cm^{-2} as described in detail below.

2.1 Microplastic samples

The study evaluated three types of microplastic polymers: PET, PP, and PE, all of which were sourced as microspheres from Lab 261 (Palo Alto, CA, USA)[27] and synthesized as additive-free, pure polymers to ensure consistent physicochemical properties relevant for environmental degradation studies. The PET (catalog number PET350K) had a nominal mean diameter of approximately 350 μm, with an estimated mean diameter of ~355 μm (coefficient of variation (CV) < 10%) and a polymer density of 1.38 g cm^{-3}. The PP (catalog number PP350K) had a nominal and actual mean diameter of approximately 350–355 μm (CV <10%) with a polymer density below 1 g cm^{-3}. The PE (catalog number PE350K) had a nominal diameter of 350 μm, an actual mean diameter of 339 μm (CV 2.26%), and a polymer density below 1 g cm^{-3}. The particles were stored at 5 °C as recommended by the manufacturer prior to UV exposures.

2.2 UV LED and far-UVC systems

Six discrete UV LED wavelengths and one far-UVC wavelength were employed in this study. Three wavelengths (268 nm, 278 nm, and 363 nm) were generated using the PearlLab Beam™ UV system (Fig. 1a, AquiSense Technologies, Erlanger, KY, USA), with advanced thermal management through stand-

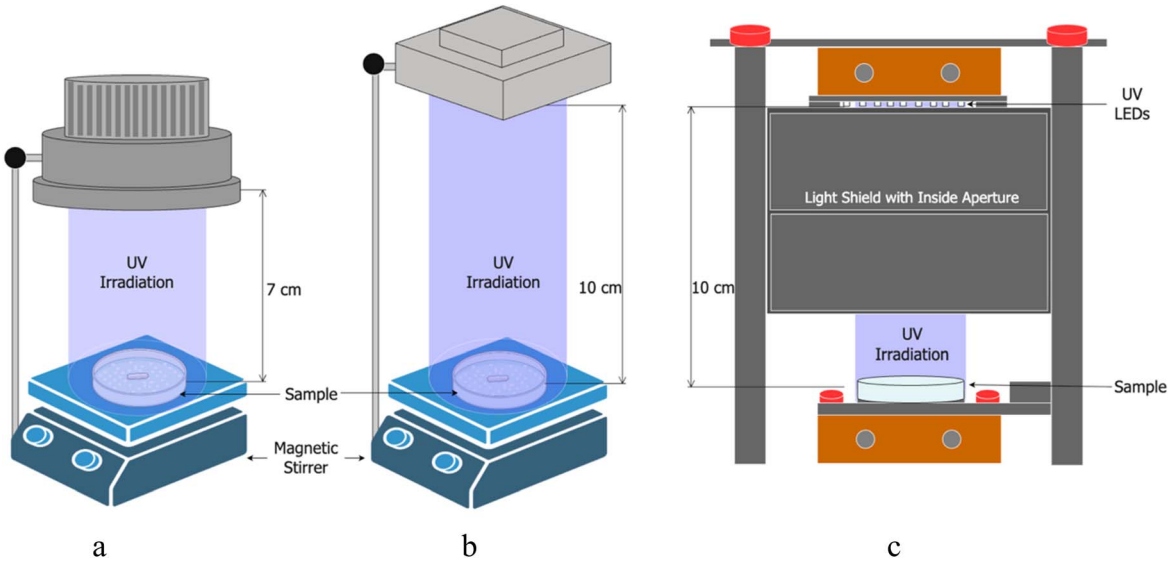

Fig. 1 Schematic representation of the three custom UV irradiation setups: (a) PearlLab Beam™ UV-LED system (268, 278, and 363 nm); (b) UVX far UV-C system (222 nm); and (c) Nichia UV-LED system (252, 290, and 300 nm).

alone cooling. The system provides precise irradiance control with instantaneous on/off capability and maintains stable UV output throughout extended exposure periods.[28] Three additional UV LED wavelengths (252 nm, 290 nm, and 300 nm) were produced using a custom water-cooled UV irradiant device developed by Nichia Corporation (Fig. 1c, Tokushima, Japan) specifically designed for UV sensitivity evaluation. This device incorporates multiple UV LED wavelengths ranging from 250–365 nm with optimized LED placement and irradiation distance to achieve highly uniform collimated light with >95% irradiance uniformity across the target area. The system features precise wavelength selectivity, stable radiant flux control, and comprehensive temperature management for both light source and sample stages.[29]

Far-UVC irradiation at 222 nm was delivered using the Zener desktop interface system (Fig. 1b, UVX Technologies, Vancouver, BC, Canada), which allows for target dose setting with real-time experiment tracking and automatic lamp shutdown upon reaching predetermined exposure levels. The experimental setups maintained consistent sample-to-source distances and incorporated appropriate safety measures including UV-opaque shielding and personal protective equipment during all irradiation procedures.[30]

2.3 UV dose determination and exposure

Accurate UV dose determination was conducted to account for variations in radiant power, radiation profile, and spectral power distribution among different UV systems and their respective wavelengths. UV LEDs were treated as polychromatic light sources, and UV dose determination was performed using radiometry. Since irradiance measurements exhibited peak values at the center of the Petri dish, the Petri factor (PF) was explicitly incorporated into the calculation of average irradiance, E_A. This calculation also included several correction factors to ensure measurement accuracy, including the reflection factor (RF) to account for light reflected at interfaces, the water factor (WF) to adjust for UV absorption by the aqueous medium, the divergence factor (DF) to correct for beam spread and geometry, and the sensor correction factor (SCF) to adjust measured irradiance by the ratio of the detector's calibrated sensitivity at the chosen wavelength to its nominal value. The SCF ensures that wavelength-dependent sensor response variations are compensated for, yielding accurate and reproducible UV dose measurements.[28,31,32] These correction factors collectively provided an accurate representation of the effective irradiance experienced by microplastic samples within the water during irradiation (eqn (1)).

$$E_A = E_0 \times PF \times RF \times WF \times DF \times SCF \quad (1)$$

Fig. 2 shows the normalized spectral output for all wavelengths tested. Corresponding Petri factors (PFs), representing irradiance uniformity across the sample area, and the full width at half maximum (FWHM) values for each source are summarized in Table 1.

To account for WF, water absorbance was measured in the sample using a Thermo Scientific NanoDrop One^c UV-Vis Spectrophotometer across the UV spectrum, from 200–400 nm. Quality control protocols ensured that samples were not allowed to settle, with vigorous mixing performed immediately prior to each measurement to maintain sample homogeneity representative of stirred UV exposure conditions. Triplicate measurements were performed for each wavelength across all three polymers (PET, PP, PE). Measured absorbance values (Table S1) were incorporated into the WF calculation and applied to eqn (1) to correct average irradiance (E_A) for wavelength dependent water sample absorbance.

Incident irradiance (E_0) was measured using an ILT 2400 radiometer equipped with wavelength-specific sensors: the SED240 sensor for wavelengths $\leq$ 300 nm and the SED005 sensor for the 363 nm wavelength. Sensors were calibrated and

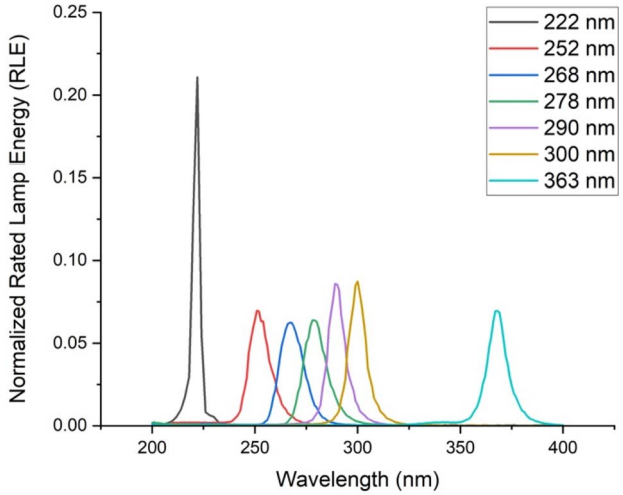

Fig. 2 Normalized spectral emission profiles of the UV sources, emitting within the UV-C to UV-A range.

Table 1 PF and FWHM values for each weighted average UV wavelength used in microplastics irradiation experiments

Wavelength (nm)	222	252	268	278	290	300	363
PF	0.98	0.98	0.98	0.98	0.97	0.97	0.95
FWHM (nm)	3.77	11.59	13.62	12.68	9.26	9.60	10.73

positioned at the same height as the microplastic samples relative to the UV LED surface, with measurements weighted at their respective weighted average wavelengths. The total UV doses (mJ cm^{-2}) applied in each experiment were determined by multiplying the average irradiance (E_A) by the irradiation time, t (sec).

Three mg of microplastic samples suspended in 5 mL of MilliQ water were placed in 35 mm diameter Petri dishes and continuously stirred using magnetic stir bars to ensure uniform exposure. Sample depth was maintained at 0.7 cm throughout all experiments. Irradiation distances were optimized for each system: 7 cm from the UV LED to the sample surface for the PearlLab Beam™ UV system, and 10 cm for both Nichia and UVX systems.

UV doses of 500, 1000, 1500, 2000, 2500, and 10 000 mJ cm^{-2} were selected to capture the progression of polymer photo-oxidation across treatment-relevant exposures. UV-AOPs in potable reuse and advanced treatment operate in the kJ cm^{-2} range, with practical applications typically occurring between 600–2000 mJ cm^{-2},[33] and recent pilot/full-scale implementations using around 1100 mJ cm^{-2}, depending on water matrix and treatment targets.[34] These values are higher than the commonly referenced 40 mJ cm^{-2} UV dose used for well-maintained drinking water UV reactors and for NSF/ANSI 55 Class A systems.[35] The initial UV dose of 500 mJ cm^{-2} represents a moderate exposure positioned just below the midpoint of typical UV-AOP operating ranges, allowing detection of early oxidative changes without excessive degradation. The incremental increases (1,00, 1,00, 2,00, 2500 mJ cm^{-2}) enable systematic tracking of oxidative functional group formation through intermediate stages of degradation. The highest UV dose (10 000 mJ cm^{-2}) corresponds to levels employed in accelerated polymer degradation research,[36] providing insight into advanced photo-oxidative aging, chain scission, and oxidative functional group formation under intensified UV exposure.

2.4 Analysis of UV-induced photodegradation

Oxidation was quantified using Carbonyl Index (CI) and Hydroxyl Index (HI) derived from FTIR spectra. Control samples of non-exposed microplastics were processed identically to UV-treated samples but without irradiation. These blanks maintained stable CI and HI throughout the experimental period, confirming baseline stability and validating UV-induced oxidation responses. For each treatment combination, 3 mg of microplastic material was prepared to enable triplicate FTIR measurements. Each UV-exposed sample was analyzed in triplicate using separate analytical subsamples drawn from the same exposed sample. For each replicate, an independent aliquot of microplastics was withdrawn from the exposed sample and analyzed with FTIR. This triplicate analytical approach accounts for analytical measurement variability, providing robust spectral precision for determining CI and HI. To evaluate between-exposure variability and justify focusing on analytical triplicates rather than replicate UV exposures, duplicate UV exposures were performed for PET at 363 nm across all UV doses. For CI, differences between duplicate exposures were small, with standard deviations ranging from 0.03 to 1.54 and corresponding coefficients of variation between 0.09% and 4.83% over all the UV doses. For HI, standard deviations were 0.03–0.07 with coefficients of variation of 1.95–4.84%. These lower variations indicate that photodegradation conditions were highly reproducible; therefore, experimental effort was directed toward analytical triplicates of independent sample of microplastics from a single well-mixed exposure for each treatment. This methodology provides robust analytical replication while maintaining consistent photodegradation conditions, following established protocols in polymer degradation research where measurement precision is prioritized through analytical replication.[35,37]

Fourier-transform infrared (FTIR) spectroscopy was used to characterize chemical changes and photo-oxidative degradation in microplastic samples following UV exposure. Spectra were collected using a Nicolet iS50 FTIR spectrometer (ThermoFisher Scientific) equipped with a diamond ATR accessory. Measurements were performed over 350–4000 cm^{-1} at 4 cm^{-1} resolution with 100 scans per spectrum. Instrument control and spectral acquisition were conducted using OMNIC software (version 9.12.928). All spectra were baseline and ATR corrected using OMNIC 9 prior to analysis. Further peak integration and analysis of spectral data were conducted in OriginPro 2024 software. The Carbonyl Index (CI) and Hydroxyl Index (HI) were determined to assess oxidative changes in microplastics following UV exposure. Both indices were calculated using the integrated

peak area under the curve for the relevant absorption bands, normalized to a reference band, following established approaches in microplastics degradation studies.[38,39] Indices were calculated as,

$$\mathrm{CI} = \frac{\mathrm{Area}_{\mathrm{carbonyl}}}{\mathrm{Area}_{\mathrm{reference}}} \quad (2)$$

$$\mathrm{HI} = \frac{\mathrm{Area}_{\mathrm{hydroxyl}}}{\mathrm{Area}_{\mathrm{reference}}} \quad (3)$$

For PET microplastics, the CI was calculated as the ratio of the integrated peak area of the carbonyl region at 1625–1770 cm^{-1} (encompassing the carbonyl C═O stretch with a peak at 1713 cm^{-1})[40] to the reference peak area at 1490–1515 cm^{-1} (aromatic ring vibration, peaking at 1505 cm^{-1}).[41,42] The HI was calculated by integrating the peak area in the 3125–3575 cm^{-1} range (O–H stretch) and normalizing to the reference peak area at 1400–1425 cm^{-1} (aromatic ring vibration, peaking at 1410 cm^{-1}).[40]

For PP microplastics, the CI was calculated as the ratio of the integrated peak area of the carbonyl region at 1650–1850 cm^{-1} (encompassing the carbonyl C═O stretch with a peak at 1727 cm^{-1}) to the reference peak area at 1417–1560 cm^{-1} (CH_3 bending vibrations, peaking at 1456 cm^{-1}).[43] The Hydroxyl Index (HI) was calculated by integrating the peak area in the 3300–3400 cm^{-1} range (O–H stretch with a peak at 3391 cm^{-1}) and normalizing to the reference peak area at 960–985 cm^{-1} (CH_3 rocking and C–C stretching vibration, peaking at 973 cm^{-1}).[4]

For PE microplastics, the CI was calculated as the ratio of the integrated peak area of carbonyl groups at 1700–1770 cm^{-1} (C═O stretch with a peak at 1734 cm^{-1})[44] to the reference peak area at 1450–1468 cm^{-1} (CH_2 scissoring vibration, peaking at 1462 cm^{-1}).[45] The Hydroxyl Index (HI) was calculated as the peak area ratio of hydroxyl groups at 3021–3353 cm^{-1} to the reference peak area at 1467–1504 cm^{-1} (corresponding to methylene (CH_2) scissoring vibration of the polymer backbone, peaking at 1472 cm^{-1}).[25,44,46]

Representative FTIR spectra for PET, PP and PE are presented in Fig. S7–S9. These spectra represent 252 nm UV exposure across the complete dose range (0–10 000 mJ cm^{-2}) and visually demonstrate the dose dependent spectral changes underlying our quantitative analysis. While raw FTIR spectra provide the complete spectral fingerprint, the calculated indices deliver quantitative degradation metrics that enable direct statistical comparison across wavelengths and polymers, which is essential for the wavelength and dose-specific degradation analysis presented in this study.

2.5 Data analysis and statistical methods

All statistical analyses and graphical presentations were performed using OriginPro 2024. The analytical approach comprised three main components: dose–response characterization, statistical significance testing, and correlation analysis. CI and HI values were plotted as functions of UV dose for each UV wavelength and polymer type to visualize oxidative trends and identify wavelength-specific response patterns. One-way analysis of variance (ANOVA) was conducted separately for each polymer–wavelength–index combination to test whether mean index values differed significantly across the six UV dose levels ($\alpha = 0.05$). Post hoc pairwise comparisons were performed using Tukey's Honest Significant Difference (HSD) test to identify which specific UV dose treatments produced significantly different oxidation indices. This analysis also assessed whether the magnitude of change in CI and HI differed considerably among the applied UV doses.

Pearson correlation analyses were performed to assess linear relationships between UV dose and the indices for each wavelength, with two-tailed p-values computed and significance evaluated at $\alpha = 0.05$. This analysis complemented the ANOVA/Tukey HSD approach by explicitly testing for monotonic dose–response trends across the experimental matrix.

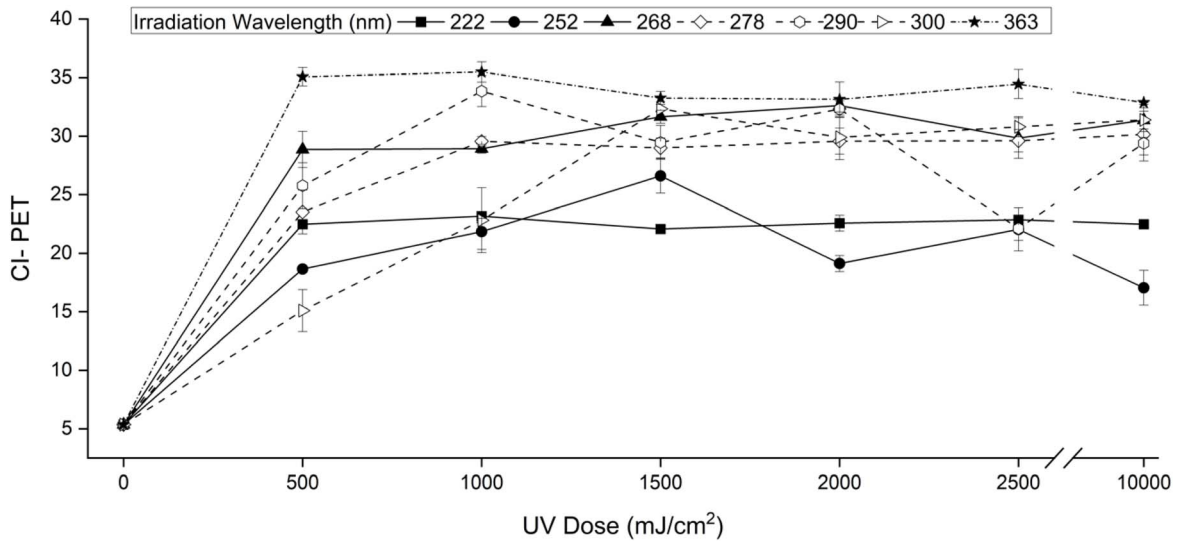

Fig. 3 Wavelength-specific and dose dependent effects of UV on PET-carbonyl index.

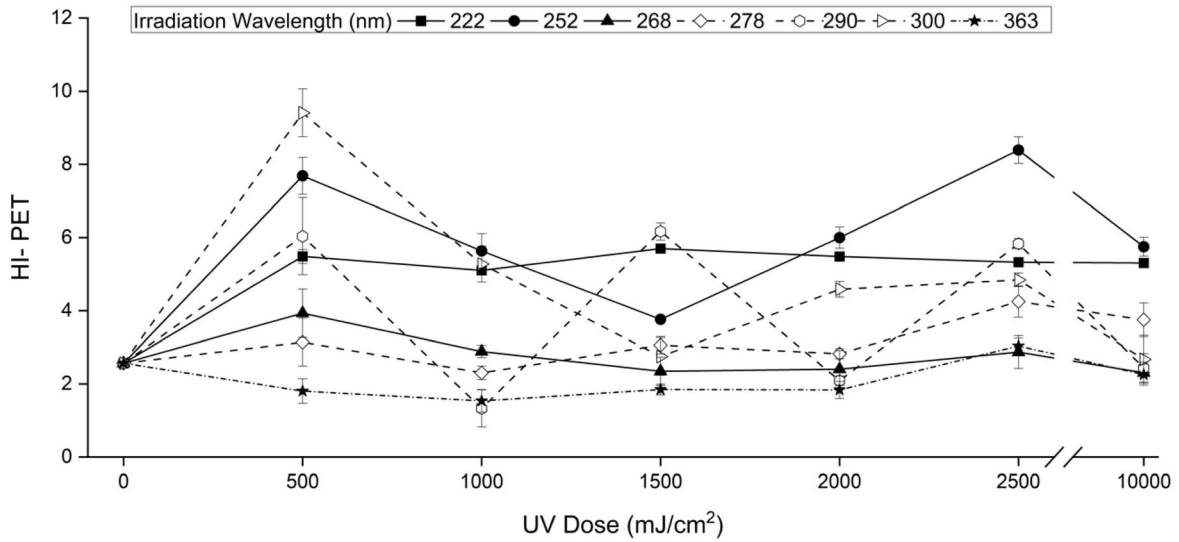

Fig. 4 Effect of UV wavelengths and doses on PET-hydroxyl index.

Additionally, Pearson correlation coefficients (r) were calculated between CI and HI values across all wavelength–dose combinations for each polymer type to quantify the strength and direction of their relationship. Correlation analyses incorporated all data points from the complete experimental matrix (7 wavelengths × 6 doses × 3 replicates per polymer). All dose–response curves included error bars representing standard error, while ANOVA results were displayed with Tukey grouping letters indicating statistical significance. This comprehensive analytical framework enabled systematic characterization of UV-induced oxidative changes and their dose, wavelength, and polymer-dependent relationships across the three microplastic types.

An important consideration for interpreting the statistical significance reported herein is that the error bars in Fig. 3–8 and the variance in ANOVA/Tukey HSD tests reflect analytical measurement variability. This analytical replication design prioritized spectral precision. Consequently, the reported p-values and confidence intervals quantify the consistency and magnitude of spectral changes within individual exposures.

3. Results and discussion

3.1 Polyethylene terephthalate (PET)

3.1.1 Carbonyl index (CI). UV irradiation of PET microplastics resulted in significant dose-dependent increases in carbonyl index (CI) across all tested wavelengths (ANOVA $p < 0.001$) above the control, demonstrating that UV exposure universally drives oxidative degradation in PET (Fig. 3). However, the rate and extent of oxidation varied significantly with spectral characteristics, reflecting distinct photochemical mechanisms.[47] At wavelengths of 222, 268, and 363 nm, CI increased rapidly from 5.36 (control) to plateau values of 22–35 by 500 mJ cm^{-2}, with Tukey's HSD grouping all UV treatments

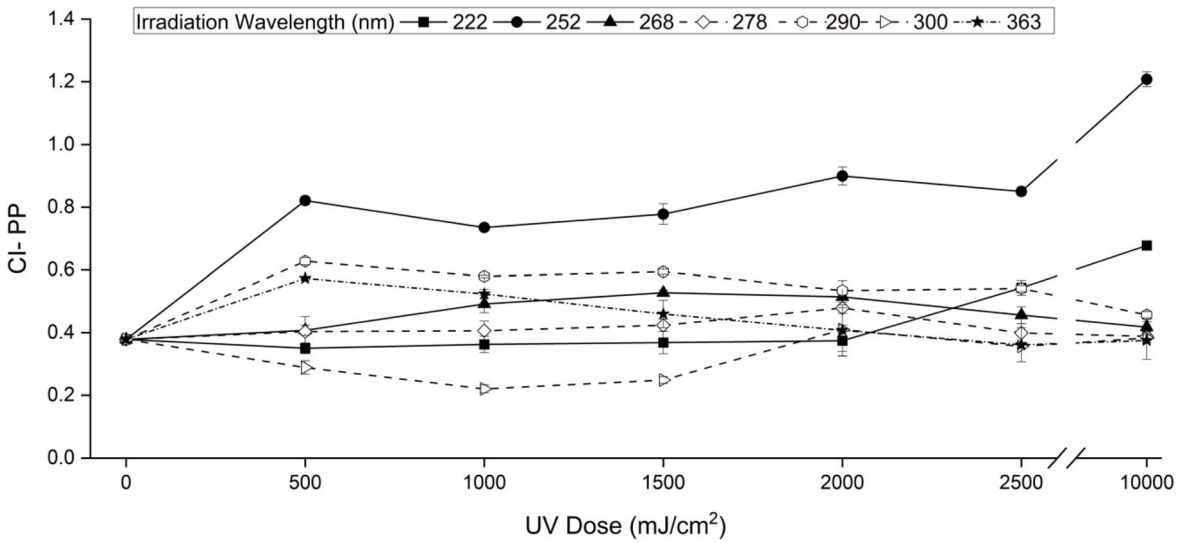

Fig. 5 Effect of UV wavelengths and doses on PP-carbonyl index.

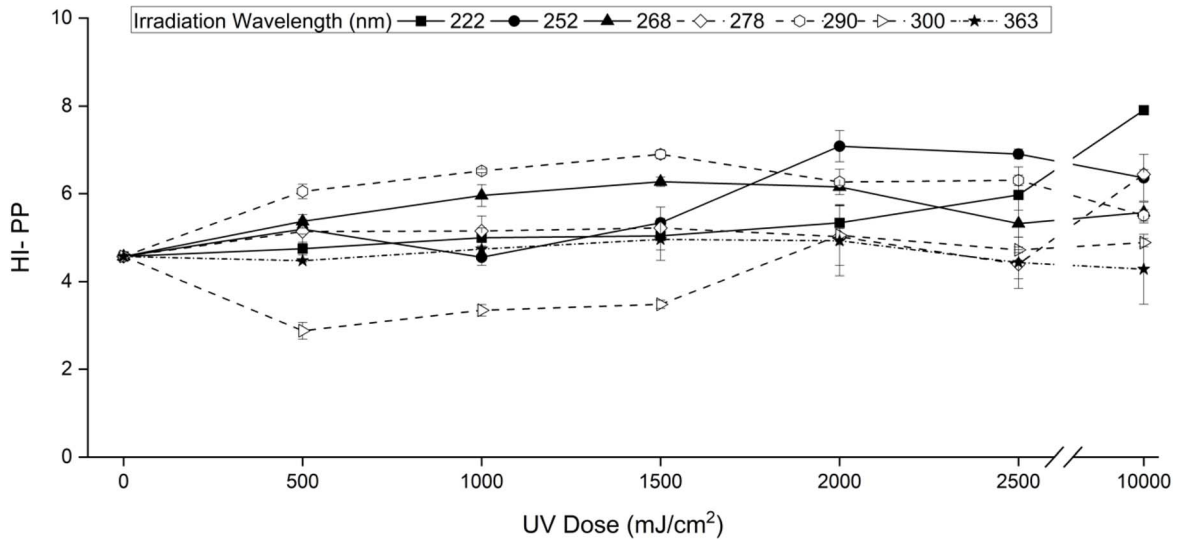

Fig. 6 Effect of UV wavelengths and doses on PP-hydroxyl index.

into a single statistical cluster distinct from controls (Table S2), indicating rapid saturation of carbonyl formation.[48]

Such rapid rise-and-plateau behavior is consistent with direct photolysis of PET ester carbonyls *via* Norrish type I (α-cleavage) and type II (γ-H abstraction/β-scission), which promptly yields radical end-groups and new carbonyls; as the most UV-labile surface sites are exhausted, additional CI growth slows toward a plateau.[40,49,50] Conversely, wavelengths 252, 278, 290, and 300 nm exhibited progressive, multi-tiered CI increases across 4–5 distinct Tukey groups, with maximum values at intermediate doses (1000–1500 mJ cm^{-2}) followed by slight declines. The non-monotonic response observed at 290 nm, where CI peaked at 33.85 (group a) at 1000 mJ cm^{-2} then declined to 22.12 (group c) at 2500 mJ cm^{-2} before rebounding, is consistent with prior PET weathering results showing temporary CI decreases under extended UV exposure and with *in situ* FTIR evidence of CO_2 evolution from PET during UV photodegradation, which can transiently lower net carbonyl signal.[40,51]

The highest CI values were observed at 363 nm (≥32.9), exceeding those at other wavelengths. In aromatic polymers such as PET, shorter-wavelength UV is strongly absorbed and therefore drives mainly surface-limited damage, whereas longer wavelengths are more weakly absorbed and can affect bulk properties when the sample is sufficiently thick; together with the fact that aromatic polymers absorb strongly above ∼290 nm and wavelength sensitivity shifts toward longer UV as thickness increases and source intensity rises with wavelength, this provides a mechanistic basis for the higher CI at 363 nm[52] (Fig. S1).

Correlation analysis between UV dose and CI at each wavelength revealed only weak to moderate relationships ($r = 0.06$–0.52, all $p > 0.2$), indicating that the dose–response curves are not strictly linear. Instead, PET CI values exhibit non-monotonic behavior, with early increases at low doses

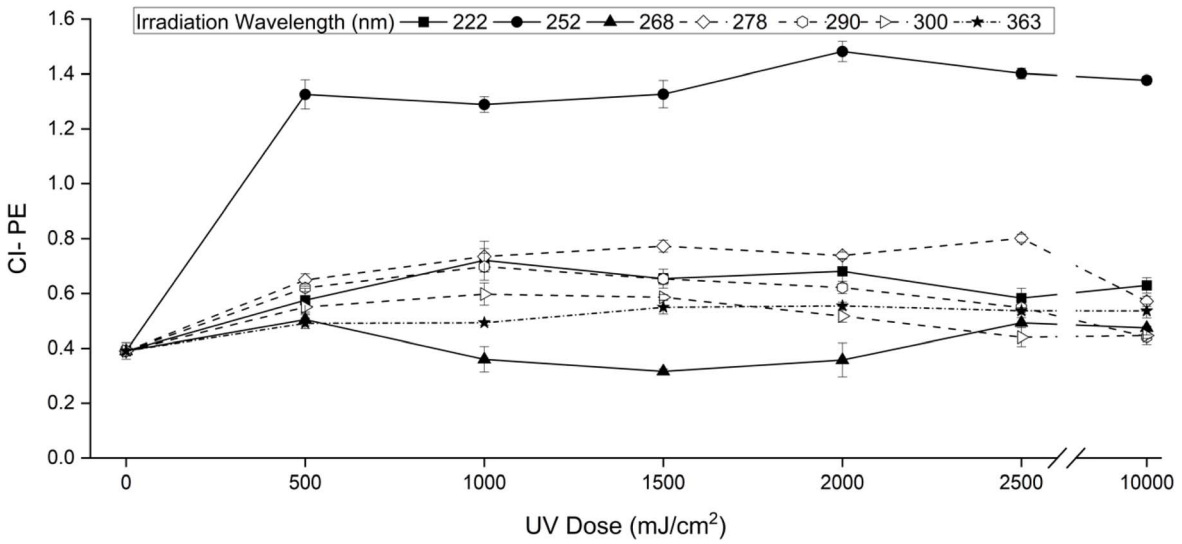

Fig. 7 Effect of UV wavelengths and doses on PE-carbonyl index.

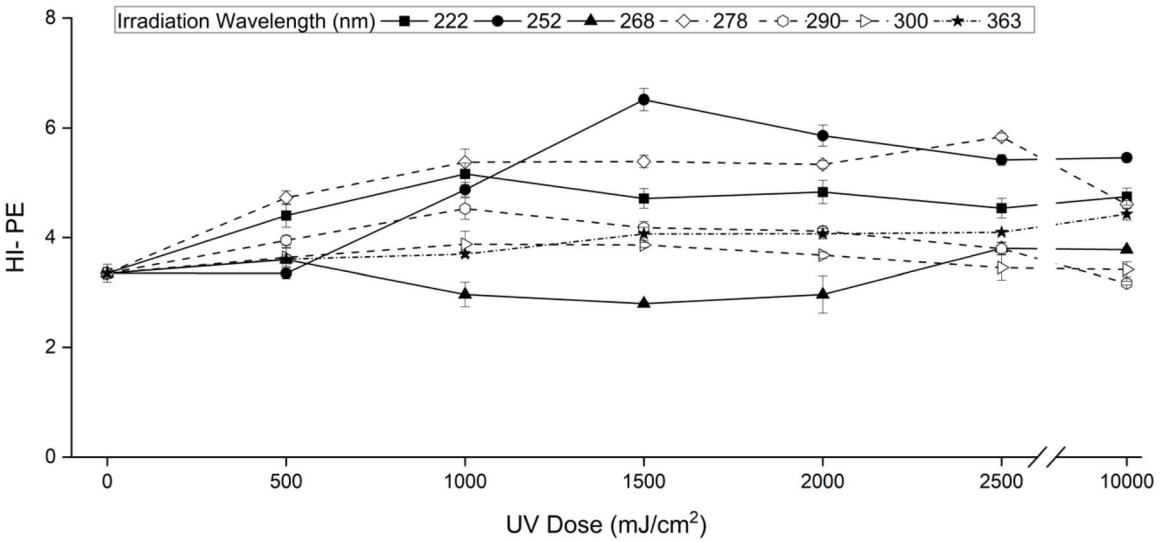

Fig. 8 Effect of UV wavelengths and doses on PE-hydroxyl index.

followed by saturation or variability at higher doses, consistent with oxidative layer buildup and self-shielding effects. The dose-wavelength response patterns of PET carbonyl index are visualized as a heatmap (Fig. S1). CI values progressively increase from baseline (5.36) at zero dose to peak intensities (>35, deep red) at higher doses, particularly under UV-A (363 nm) and mid-UV wavelengths (268–290 nm). In contrast, shorter UV-C wavelengths (222–252 nm) generally show lower CI intensities (blue to pale red, <20) across most doses. This pattern highlights the stronger oxidative responses concentrated in longer wavelengths despite their lower photon energy.

3.1.2 Hydroxyl index (HI). The systematic analysis of PET microplastics exposed to varying UV wavelengths (222–363 nm) and doses (0–10 000 mJ cm^{-2}) revealed significant wavelength and dose-dependent effects on HI formation, often exhibiting non-monotonic responses with dose and clear deviations from linear dose-response relationships (Fig. 4). UV radiation at 300 nm demonstrated the highest degradation efficiency (maximum HI = 9.41), followed by 252 nm (HI = 8.39) and 290 nm (HI = 6.17), consistent with previous findings that UV-B wavelengths (280–315 nm) cause the highest degree of PET degradation through chain scission of the ester bonds in the PET backbone.[40]

Notably, the 500 mJ cm^{-2} dose produced the highest overall mean hydroxyl index (5.36 ± 2.45); although this response was highly wavelength-dependent, with six wavelengths showing increased degradation, 363 nm exhibited reduced hydroxyl formation (HI = 1.80) below baseline levels (HI = 2.57), indicating wavelength-specific photochemical mechanisms rather than uniform UV effects. Higher doses consistently showed diminished effectiveness across wavelengths, demonstrating non-linear photochemical kinetics with dose-dependent saturation effects rather than simple linear relationships. One-way ANOVA with Tukey's HSD demonstrated statistically significant differences among UV doses within each wavelength ($p < 0.05$) except at 363 nm (Table S3), yet no significant linear correlations were observed between dose and HI formation ($r =$ −0.42 to +0.54, $p = 0.21$–0.75), suggesting that PET degradation involves threshold effects and competing photochemical processes.

The dose-wavelength response patterns of PET hydroxyl index are visualized as a heatmap (Fig. S2), showing heterogeneous and wavelength-dependent behavior. Weak and inconsistent correlations with dose ($r = -0.42$ to 0.54, all $p > 0.2$) indicate that HI changes were non-linear and often non-monotonic. Some wavelengths (*e.g.*, 278 nm, $r = 0.54$) suggested moderate dose dependence, while others (*e.g.*, 268 nm, $r = -0.42$) showed inverse or fluctuating trends. The highest HI values (red, >7.0) occurred sporadically at 252 and 300 nm under specific doses, while most other wavelengths, including 268–290 nm and 363 nm, exhibited lower intensities (blue to light blue, <3.0). This indicates that hydroxyl formation in PET is irregular and does not follow a uniform dose-dependent trend across the UV spectrum. Overall, HI did not follow a simple linear dose–response, consistent with competing, wavelength-dependent oxidative pathways in PET. The patterns likely reflect the formation and subsequent transformation of O–H bearing oxidation products (*e.g.*, alcohols/hydroperoxides) rather than monotonic accumulation.

Sample temperature was monitored during the longest irradiation condition (10 000 mJ cm^{-2}) for both UV-A and UV-C exposures. No measurable temperature increase was observed, and the aqueous suspension remained below 20 °C during irradiation for both wavelengths. Therefore, the observed CI and HI changes are attributed to UV-driven photochemical oxidation rather than temperature-assisted hydrolytic processes. Under room temperature and atmospheric pressure conditions, neutral-pH aqueous conditions without heat or catalysts, hydrolysis of PET is negligible. Substantial hydrolysis rates are only achieved under severe processing conditions, including temperatures between 190 to 400 °C and pressures ranging from 1 to 35 MPa.[53] Similarly, chemical hydrolysis of polyesters at ambient conditions (20 to 37 °C) is extremely slow, with meaningful hydrolysis only achieved at elevated

temperatures exceeding 50 to 60 °C.[54] Furthermore, in our methodology, the post-exposure sample preparation involved drying for 48 hours in a desiccator at room temperature under low relative humidity (<30%), which halts water mediated hydrolytic reactions and ensures FTIR spectra represent photochemically oxidized products. Collectively, these observations confirm that photochemical oxidation is the dominant degradation pathway measured in this work.

3.2 Polypropylene (PP)

3.2.1 Carbonyl index (CI). PP microplastics produced significant, wavelength-dependent changes in the CI across 0–10 000 mJ cm^{-2} (ANOVA $p < 0.001$; Tukey HSD, Table S4). At 222 nm, CI rose sharply from 0.38 (control) to 0.54 by 2500 mJ cm^{-2} and 0.68 at 10 000 mJ cm^{-2}, forming a distinct cluster (group a) that plateaued only at the highest dose. Similarly, 252 nm treatment yielded CI values of 0.82 at 500 mJ cm^{-2} and 1.21 at 10 000 mJ cm^{-2}, demonstrating progressive oxidation with no clear saturation. In contrast, intermediate wavelengths (268, 278, 290 nm) exhibited multi-tiered CI increases, peaking at 1500 or 2000 mJ cm^{-2} before slight declines at higher doses (Fig. 5), similar to,[55] indicative of non-monotonic behavior likely due to competing cross-linking or radical termination processes. Wavelengths 300 and 363 nm showed minimal CI change (0.22–0.41 across all doses), consistent with lower photon energy insufficient for extensive ester oxidation. The dose-wavelength CI response patterns are visualized as a heatmap (Fig. S3), clearly showing the highest CI values (red, >1.0) concentrated at 252 nm across intermediate to high doses, while shorter wavelengths (222 nm) and longer wavelengths (300–363 nm) exhibited more moderate responses (blue to light blue, <0.7).

Statistically significant positive correlations were observed at 222 nm ($r = 0.91$, $p = 0.0045$) and 252 nm ($r = 0.82$, $p = 0.0227$), indicating strong linear relationships between UV dose and CI at these wavelengths. In contrast, correlations at other wavelengths were weak and non-significant: 268 nm ($r = -0.13$, $p = 0.787$), 278 nm ($r = -0.17$, $p = 0.720$), 290 nm ($r = -0.28$, $p = 0.536$), 300 nm ($r = 0.38$, $p = 0.405$), and 363 nm ($r = -0.43$, $p = 0.333$). The variation in both magnitude and direction of correlation coefficients across wavelengths suggests that dose-response relationships are not uniform across the UV spectrum studied (Table S8). Additionally, these findings demonstrate that wavelength selection critically determines dose–response predictability in PP photodegradation, with shorter UV wavelengths promoting consistent carbonyl formation while longer wavelengths result in non-monotonic degradation patterns.

3.2.2 Hydroxyl index (HI). Pearson correlation analysis ($n = 7$ per wavelength) revealed a very strong, significant positive dose-HI relationship at 222 nm ($r = 0.983$, $p < 0.0001$) and a moderate, significant relationship at 278 nm ($r = 0.828$, $p = 0.0215$). All other wavelengths showed weak, non-significant correlations (252 nm: $r = 0.296$, $p = 0.519$; 268 nm: $r = 0.110$, $p = 0.814$; 290 nm: $r = -0.131$, $p = 0.780$; 300 nm: $r = 0.473$, $p = 0.284$; 363 nm: $r = -0.529$, $p = 0.222$), indicating inconsistent or non-monotonic HI responses (Fig. 6). In contrast Alavian Petroody[56] observed greater CI and HI formation under UV-A in polypropylene within biosolid suspensions, our study in a clean aqueous medium demonstrates the opposite trend, with a strong linear HI increase at 222 nm driven by efficient photon absorption and chain scission. The dose-wavelength HI response patterns are visualized as a heatmap (Fig. S4), revealing peak HI values (red, >7.0) at 222 nm and 252 nm at high doses (2500–10000 mJ cm^{-2}), while 300 nm consistently exhibited the lowest HI values (blue, <3.5) across all doses, confirming wavelength-dependent hydroxyl formation in PP.

When limiting the UV dose range to 0–1500 mJ cm^{-2} ($n = 4$ per wavelength), Pearson correlations between dose and PP-Hydroxyl Index (HI) were highly significant at 222 nm ($r = 0.971$, $p = 0.029$), 268 nm ($r = 0.982$, $p = 0.018$), and 290 nm ($r = 0.969$, $p = 0.030$). A positive but weaker correlation was observed at 278 nm ($r = 0.909$, $p = 0.091$), while correlations at 252 nm, 300 nm, and 363 nm were weaker and non-significant ($r = 0.522$–0.870, $p = 0.130$–0.704), indicating more variable HI responses in that dose window. Restricting analysis to ≤1500 mJ cm^{-2} captures the initial, near-linear phase of hydroxyl formation, revealing that UV wavelengths of 222 nm, 268 nm, 278 nm, 290 nm drive consistent HI increases (Table S5). This focused range is thus appropriate for quantifying intrinsic dose–response sensitivity, while higher doses are needed to evaluate saturation or secondary photochemistry.

3.3 Polyethylene (PE)

3.3.1 Carbonyl index (CI). PE microplastics exhibited pronounced, wavelength-dependent changes in CI across 0–10 000 mJ cm^{-2} UV doses (ANOVA; Tukey HSD, Table S6). At 252 nm, PE-CI values rose sharply from 0.39 (control) to 1.33 by 1500 mJ cm^{-2}, peaking at 1.48 at 2000 mJ cm^{-2} before plateauing (CI 1.38–1.40) at higher doses, forming a distinct high-CI cluster (Group a, Table S6). This pronounced and sustained increase at 252 nm reflected efficient photooxidation, consistent with maximal photon energy absorption leading to persistent carbonyl formation.

In contrast, irradiation at 222 nm produced less marked increases (CI 0.39 to 0.68) with a modest plateau forming beyond 2000 mJ cm^{-2} (CI ~0.6), suggesting surface passivation or effects related to the penetration depth. Wavelengths 268, 278 nm demonstrated multi-tiered CI increases, indicative of non-monotonic oxidation (Fig. 7). These patterns mirror the behavior seen in previous studies,[55] where limited chain mobility or radical termination processes skate the balance between carbonyl accrual and molecular rearrangement at moderate energies. Wavelengths 290, 300, and 363 nm delivered consistently lower CI values (0.39–0.70), with only marginal increases across the entire dose range (Fig. S5 and Table S6), consistent with insufficient photon energy to drive extensive carbonyl formation *via* Norrish Type I or II processes.

Pearson correlation analysis (Table S8) revealed that dose-dependent CI trends were not statistically significant across any wavelength examined. Correlations were weak to moderate but non-significant: 252 nm ($r = 0.35$, $p = 0.44$), 222 nm ($r = 0.23$, $p = 0.61$), 268 nm ($r = 0.35$, $p = 0.45$), 278 nm ($r = -0.08$, $p = 0.87$), 290 nm ($r = -0.39$, $p = 0.38$), 300 nm ($r = -0.29$, $p =$

0.53), and 363 nm ($r = 0.55$, $p = 0.20$). The diversity of correlation coefficients—spanning weak positive to moderate negative values, combined with the lack of statistical significance highlights the absence of clear linear dose-response relationships across the UV spectrum for PE microplastics.

While 252 nm produced the highest CI values (1.48), the absence of significant dose–response correlations across wavelengths indicates PE photodegradation follows complex, non-linear pathways. The elevated CI at 252 nm reflects optimal photon energy for C–H abstraction and carbonyl formation, but competing processes (cross-linking, radical termination, surface passivation) disrupt linear dose-dependence. All wavelengths showed non-significant correlations, suggesting simultaneous photochemical pathways and wavelength-dependent magnitude differences without dose-predictability, indicating non-linear degradation kinetics rather than straightforward dose-response relationships.

3.3.2 Hydroxyl index (HI). UV irradiation produced a clear wavelength- and dose-dependent increase in HI. By 500 mJ cm^{-2}, HI rose modestly at most wavelengths but increased markedly at 252 nm (3.60) and 278 nm (4.73). Peak HI occurred at 1000, 1500 mJ cm^{-2} under high-energy UV (222, 252, 278 nm), with 252 nm reaching a maximum HI of 6.51 at 1500 mJ cm^{-2} before declining to 5.46 at 10 000 mJ cm^{-2}. In contrast, wavelengths 290, 300 and 363 nm yielded minimal HI enhancements ($\leq$4.06) across the entire dose range (Fig. 8 and Table S7). The heatmap (Fig. S6) highlighted two hot spots of maximal HI at 252 nm/1500 mJ cm^{-2} and 278 nm/2500 mJ cm^{-2}, whereas 268 nm consistently delivered the lowest HI values at higher doses. These findings indicate wavelength dependant HI formation in PE. The observed plateau and subsequent HI decrease at high doses likely reflect competing radical recombination and crosslinking, which inhibit further functionalization.

Only the 363 nm irradiation exhibited a statistically significant positive correlation between UV dose and hydroxyl index ($r = 0.80$, $p = 0.032$), indicating a clear, dose-dependent increase in HI. In contrast, wavelengths 222 to 278 nm showed weak to moderate but non-significant positive correlations ($r = 0.03$–0.47), reflecting non-linear dose–response behavior, and UV 290 and 300 nm yielded negative correlations ($r = -0.57$ to -0.35), suggesting competing processes such as crosslinking reduce hydroxyl formation at higher doses.

3.4 Correlation between CI and HI

Across all wavelengths and doses, PET exhibited a weak but statistically significant inverse relationship between carbonyl and hydroxyl indices ($r = -0.197$, $p = 0.0166$; $n = 147$), with higher HI values tending to coincide with slightly lower CI values (Fig. 9 and Table S9). This inverse association is consistent with PET's stage-wise photo-oxidative conversion, wherein early OH-/hydroperoxide-bearing intermediates accumulate and subsequently undergo secondary reactions and chain scission to carboxyl/carbonyl products, leading to HI stabilization or decline as CI increases.[40,49]

A moderate positive correlation ($r = 0.354$, $p < 0.0001$, $n = 147$) between CI and HI in PP microplastics degradation, indicates a significant linear relationship between these two oxidative degradation indicators (Fig. 9 and Table S9). This correlation aligns with established degradation mechanisms in PP photooxidation, where both carbonyl (C═O) and hydroxyl (O–H) functional groups are formed simultaneously through free radical oxidation processes.[57] The observed relationship reflects the complex oxidative degradation pathway where hydroperoxides (ROOH), formed during the initial stages of PP degradation, decompose to generate both hydroxyl radicals and alkoxy radicals, subsequently leading to the formation of carbonyl groups through β-scission reactions and hydroxyl groups through hydrogen abstraction.[58] The moderate correlation coefficient ($r = 0.354$) suggests that while CI and HI development follow similar oxidative pathways, they may be influenced by different kinetic factors during the degradation process. The significant positive correlation ($p < 0.0001$) confirms that both functional groups serve as reliable indicators of PP microplastic weathering, with their co-development reflecting the extent of surface oxidation and polymer chain scission occurring during environmental degradation processes.

A strong positive correlation ($r = 0.733$, $p < 0.0001$, $n = 147$) between CI and HI in PE microplastics degradation, indicates a highly significant linear relationship between these two oxidative degradation indicators (Fig. 9 and Table S9). This strong correlation demonstrates that both carbonyl (C═O) and hydroxyl (O–H) functional groups are formed simultaneously during photooxidation processes.[59] This strong positive correlation reflects interconnected oxidative degradation pathways

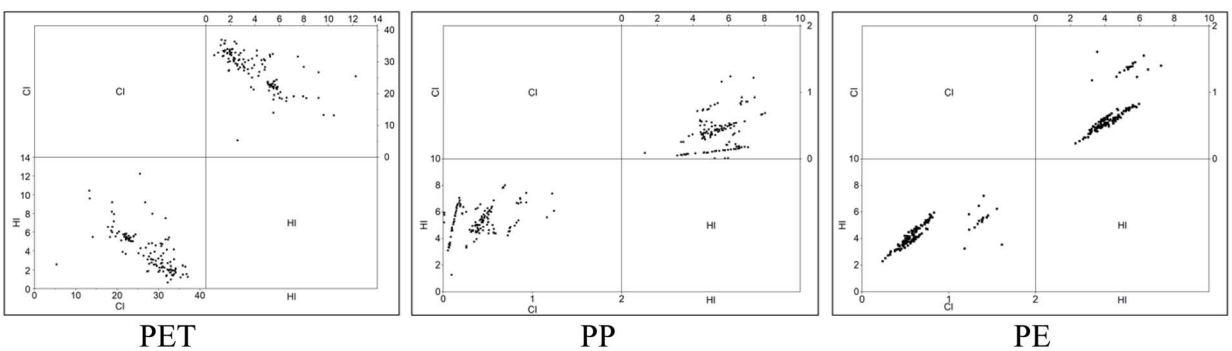

Fig. 9 Relationship between UV-induced changes to the CI and HI in PET, PP, and PE microplastics.

where hydroperoxides (ROOH), formed during PE degradation, decompose through multiple parallel routes that simultaneously generate both carbonyl groups through β-scission and ketone formation and hydroxyl groups through alcohol formation and hydroxyl radical reactions.[52,58]

The correlation strength suggests that PE undergoes comprehensive surface oxidation where multiple oxidative processes occur simultaneously, with both CI and HI increasing progressively through parallel degradation routes. The highly significant positive correlation ($p < 0.0001$) confirms that both functional groups serve as reliable and correlated indicators of PE microplastic environmental degradation, with their strong co-development pattern reflecting the extent of synchronized surface oxidation processes occurring in PE microplastics during aging.

3.5 Polymer intrinsic UV response: mechanistic baseline and environmental context

This study employs a synthetic, additive-free microplastic model designed to isolate the intrinsic photochemical behavior of pure polymers under controlled UV wavelengths. The size range (300–500 μm) is environmentally relevant, representing the microplastic class most commonly encountered in aquatic and wastewater systems. While this approach differs from environmental microplastics, which are inherently heterogeneous and contain processing additives, the synthetic model serves a critical mechanistic function. Environmental microplastics are confounded by multiple overlapping factors: (1) mixed polymer types with overlapping FTIR absorption bands;[60] (2) processing aids (UV absorbers, antioxidants, plasticizers) that directly alter photodegradation pathways;[61] (3) pigments that affects the light absorption;[62] and (4) pre-existing morphological weathering that affects reactivity.[63] These confounding factors make wavelength and dose-specific UV effects impossible to quantify in real environmental samples. Accordingly, our research provides quantitative baseline data on polymer-intrinsic photochemistry. The CI and HI reported herein can be used to calibrate more sophisticated models of microplastic degradation in complex environmental systems where additives and heterogeneity are present. Future studies should systematically investigate the modulatory effects of processing aids, mixed polymers, and environmental aging on the wavelength-specific degradation kinetics characterized in this idealized system.

Degradation indicators such as CI and HI derived from laboratory weathering experiments should not be directly equated with those measured in environmental samples, as laboratory experiments are typically conducted under tightly controlled conditions. This isolates the effects of a specific factor while excluding other variables present in natural systems. Nevertheless, field observations also show differences in these indicators. For example, when 2950 PE and PP microplastics collected from coastal waters around Japan were analyzed, the mean CI values were 0.69 ± 0.34 for PE and 0.70 ± 0.34 for PP. Overall, the authors found no significant differences in CI across color or shape, but CI was significantly lower for green PE and higher for white PE fibers compared to fragments. They also reported a significant negative correlation between the station-averaged CI and particle length for white PE fragments, indicating that smaller particles tend to be more oxidized and therefore more deteriorated after longer exposure in the marine environment.[38] Artificially UV-aged PE, PP, and Polystyrene (PS) were compared, with environmental analysis focused on PE microplastics collected from freshwater. FTIR-based degradation indices increased with irradiation time during laboratory experiments and show characteristics corresponding to greater degradation with residence time in the environment.[44] Several plastic polymer types were also aged *in situ* in marine surface waters for 12 months. Significant increases in HI and CI were reported for certain weathered polymers such as polyaramid (PA), and the ageing indices showed non-linear changes similar to those observed in our study[64]

Thus, while both environmental and laboratory aged microplastics exhibit similar trends in degradation indices, values in aquatic environmental samples are additionally shaped by factors such as polymer chemistry and the presence of additives, alongside interacting environmental variables including light intensity and UV radiation, exposure duration, temperature, pH, oxygen availability and nutrient availability, water depth, wave action, and biofilm formation.[65] Laboratory experiments conducted under controlled conditions are, therefore best interpreted as mechanistic indicators of specific effect rather than as directly comparable to field samples.

4. Conclusions

Using discrete UV LED (252, 268, 278, 290, 300, 363 nm) and far-UVC (222 nm) wavelengths, multi-wavelength, dose-controlled (500–10 000 mJ cm^{-2}) comparison across PET, PP, and PE microplastics shows that photo-oxidation is strongly wavelength-selective, polymer-specific, and frequently non-linear with UV dose.

For PET, HI was heterogeneous and dose-non-monotonic, with pronounced hotspots near 252 nm (8.39) 300 nm (9.41) and, while 363 nm reduced HI below baseline, yet UV-A at 363 nm produced the highest CI (>32.9), consistent with deeper UV-A penetration and bulk-biased oxidation in thicker aromatic polymers. PET exhibited rapid CI saturation, reaching plateau values by 500 mJ cm^{-2}, while wavelengths of 252 to 300 nm showed multi-tiered, non-monotonic responses due to competing photochemical pathways. Pooled PET data yielded a weak but significant inverse CI–HI relationship ($r = -0.197$), indicating stage-wise oxidation in which hydroxyl-type intermediates do not rise proportionally as carbonyls accumulate.

For PP, dose response behavior depended on both wavelength and the index. HI rose with dose at 222 nm ($r = 0.983$, $p < 0.0001$) and moderately at 278 nm ($r = 0.828$, $p = 0.0215$), while HI-dose relationships were weak or non-significant at 252, 268, 290, 300, and 363 nm, indicating wavelength-dependent and often inconsistent hydroxyl formation. For CI, significant positive dose correlations occurred at 222 nm ($r = 0.91$, $p = 0.0045$) and 252 nm ($r = 0.82$, $p = 0.0227$) with maximum CI of 1.21 at 252 nm; other wavelengths showed weak, non-significant

relationships with wavelengths 268 to 290 nm exhibiting multi-tiered CI increases. Across all tested wavelengths and doses, CI and HI were positively correlated in PP ($r = 0.354$, $p < 0.0001$; $n = 147$), indicating a moderate co-evolution of carbonyl and hydroxyl functional groups through concurrent free-radical oxidation pathways.

For PE, HI was wavelength dependent. The UV dose and the HI relationship was strong and significant at 363 nm ($r = 0.796$, $p = 0.032$), but weak or non-significant at 222, 252, 268, 278, 290, and 300 nm. For CI, correlations with dose were weak to moderate and non-significant at all wavelengths. However, the 252 nm yielded the highest CI (1.48) and HI (6.51) values. When aggregated over all wavelengths and doses, CI and HI were strongly and positively correlated in PE ($r = 0.733$, $p < 0.0001$; $n = 147$), indicating synchronous growth of oxygenated functionalities under UV exposure through parallel degradation routes forming both carbonyl and hydroxyl groups simultaneously.

Across all three polymers, UV exposure produced measurable changes relative to unexposed controls as quantified by ATR-FTIR spectroscopy using polymer-specific wavelength ranges for CI and HI determination. PET showed CI increases across wavelengths (highest at 363 nm) with within-wavelength HI differences despite non-linearity; PP showed CI gains at 222 and 252 nm with HI strongest at 222 nm; and PE showed the highest CI at 252 nm (followed by a plateau) with HI increases at several wavelengths, notably 252–278 nm.

Together, these results demonstrate that (i) UV wavelength is a prominent influence on oxidation pathways that interacts with dose and polymer chemistry of PET, PP and PE (ii) CI and HI are complementary, not interchangeable indicators; their relationship depends on polymer chemistry (inverse for PET, moderate positive for PP, strong positive for PE), and (iii) dose–response behavior frequently deviates from linearity, especially for PET, implying thresholds and competing kinetics. These findings provide critical quantitative data for improving predictive models of microplastic persistence, surface reactivity, and environmental fate in aquatic systems and water treatment applications.

Compared with previous studies, we used six discrete UV LED wavelengths (252, 268, 278, 290, 300, 363 nm) plus far-UVC (222 nm) to quantify wavelength and dose-dependent degradation in PET, PP, and PE microplastics; to our knowledge, this is the first study to span this full set of wavelengths across these polymers. Future work should integrate these wavelength-specific degradation kinetics into environmental risk assessments, quantify chemical leaching patterns associated with wavelength-specific oxidative changes, and explore effects of UV wavelengths on weathering.

Author contributions

TR: conceptualization, experimental design and investigation, data collection, analysis, and visualization; manuscript writing and revising. PON: methodology, experimental guidance; results interpretation, manuscript reviewing and editing. SEB: funding acquisition, project administration and supervision, experimental guidance, validation, manuscript reviewing and editing.

Conflicts of interest

There are no conflicts to declare.

Data availability

The data supporting this article have been included as part of the supplementary information (SI). Supplementary information: water absorbance and water-factor calculations, ATR-FTIR-derived carbonyl and hydroxyl indices for PET, PP, and PE across seven UV wavelengths and UV doses (0–10 000 mJ cm^{-2}) with Tukey HSD groupings, heatmaps, and Pearson correlation analyses, plus representative ATR-FTIR spectra. See DOI: https://doi.org/10.1039/d5em00818b.

Acknowledgements

This work was supported by the Natural Sciences and Engineering Research Council of Canada *via* NSERC Discovery Grant (RGPIN-2021-03560), NSERC CREATE Program grant (565088-2022), and NSERC Postgraduate Scholarship-Doctoral (PGS D 601229-2025) to TR, as well as the National Research Council Canada (NRC) Ocean Program (#OCN-708-1). We thank Dr Obinna Onuaguluchi (Structural Materials Engineering Laboratory, UBC) for assistance with FTIR analysis, Felix Shuen and Brad Wishart (Environmental Systems Engineering Laboratory, UBC) for support with laboratory operations, and Dr Anusha Perera for guidance on statistical tools and data interpretation. We acknowledge Nichia for loaning the UV LED irradiance device and Todd Mikowski for technical support. The authors also thank Dr Loretta Li (Department of Civil Engineering, UBC) and Dr Maria E. Holuszko (Department of Mining Engineering, UBC) for serving on the research committee and providing constructive guidance and feedback.

References

1 R. Geyer, J. R. Jambeck and K. L. Law, Production, use, and fate of all plastics ever made, *Sci. Adv.*, 2017, **3**, e1700782.
2 K. Houssini, J. Li and Q. Tan, Complexities of the global plastics supply chain revealed in a trade-linked material flow analysis, *Commun Earth Environ.*, 2025, **6**, 257.
3 M. Cole, P. Lindeque, C. Halsband and T. S. Galloway, Microplastics as contaminants in the marine environment: a review, *Mar. Pollut. Bull.*, 2011, **62**(12), 2588–2597.
4 S. Veerasingam, M. Ranjani, R. Venkatachalapathy, A. Bagaev, V. Mukhanov, D. Litvinyuk, *et al.*, Contributions of Fourier transform infrared spectroscopy in microplastic pollution research: A review, *Crit. Rev. Environ. Sci. Technol.*, 2021, **51**(22), 2681–2743.
5 X. Li, X. Shen, W. Jiang, Y. Xi and S. Li, Comprehensive review of emerging contaminants: Detection technologies, environmental impact, and management strategies, *Ecotoxicol. Environ. Saf.*, 2024, **278**, 116420.
6 OECD, *Policies to Reduce Microplastics Pollution in Water: Focus on Textiles and Tyres*. OECD Publishing, 2021, DOI: 10.1787/7ec7e5ef-en.

7 C. Campanale, G. Dierkes, C. Massarelli, G. Bagnuolo and V. F. Uricchio, A relevant screening of organic contaminants present on freshwater and pre-production microplastics, *Toxics*, 2020, **8**(4), 100.
8 J. Lorenzo-Navarro, M. Castrillon-Santana, E. Sanchez-Nielsen, B. Zarco, A. Herrera, I. Martinez, *et al.*, Deep learning approach for automatic microplastics counting and classification, *Sci. Total Environ.*, 2021, **765**, 142728.
9 A. Turner and M. Filella, Hazardous metal additives in plastics and their environmental impacts, *Environ. Int.*, 2021, **156**, 106622.
10 A. A. Yusuf, J. D. Ampah, M. E. M. Soudagar, I. Veza, U. Kingsley, S. Afrane, *et al.*, Effects of hybrid nanoparticle additives in n-butanol/waste plastic oil/diesel blends on combustion, particulate and gaseous emissions from diesel engine evaluated with entropy-weighted PROMETHEE II and TOPSIS: Environmental and health risks of plastic waste, *Energy Convers. Manage.*, 2022, **264**, 115758.
11 P. Liu, X. Zhan, X. Wu, J. Li, H. Wang and S. Gao, Effect of weathering on environmental behavior of microplastics: Properties, sorption and potential risks, *Chemosphere*, 2020, **242**, 125193.
12 A. Paluselli, V. Fauvelle, F. Galgani and R. Sempere, Phthalate release from plastic fragments and degradation in seawater, *Environ. Sci. Technol.*, 2018, **53**(1), 166–175.
13 I. Savino, C. Campanale, P. Trotti, C. Massarelli, G. Corriero and V. F. Uricchio, Effects and impacts of different oxidative digestion treatments on virgin and aged microplastic particles, *Polymers*, 2022, **14**(10), 1958.
14 J. Almond, P. Sugumaar, M. N. Wenzel, G. Hill and C. Wallis, Determination of the carbonyl index of polyethylene and polypropylene using specified area under band methodology with ATR-FTIR spectroscopy, *E-Polym.*, 2020, **20**(1), 369–381.
15 Y. Dong, M. Gao, Z. Song and W. Qiu, As (III) adsorption onto different-sized polystyrene microplastic particles and its mechanism, *Chemosphere*, 2020, **239**, 124792.
16 P. Liu, L. Qian, H. Wang, X. Zhan, K. Lu, C. Gu, *et al.*, New insights into the aging behavior of microplastics accelerated by advanced oxidation processes, *Environ. Sci. Technol.*, 2019, **53**(7), 3579–3588.
17 J. Brandon, M. Goldstein and M. D. Ohman, Long-term aging and degradation of microplastic particles: comparing *in situ* oceanic and experimental weathering patterns, *Mar. Pollut. Bull.*, 2016, **110**(1), 299–308.
18 S. E. Beck, N. M. Hull, C. Poepping and K. G. Linden, Wavelength-Dependent Damage to Adenoviral Proteins Across the Germicidal UV Spectrum, *Environ. Sci. Technol.*, 2018, **52**(1), 223–229.
19 I. I. Blatchley, D. J. Brenner, H. Claus, T. E. Cowan, K. G. Linden, Y. Liu, *et al.*, Far UV-C radiation: An emerging tool for pandemic control, *Crit. Rev. Environ. Sci. Technol.*, 2023, **53**(6), 733–753.
20 Y. Liu and N. M. Hull, Emerging investigator series: Inactivation of antibiotic resistant bacteria and inhibition of horizontal resistance gene transfer is more effective by 222 than 254 nm UV, *Environ. Sci.:Water Res. Technol.*, 2025, **11**(2), 306–316.
21 D. McDonald, D. Ma and N. M. Hull, 222 nm causes greater protein damage and repair inhibition of E. coli than 254 nm for water disinfection, *PLOS Water*, 2024, **3**(7), e0000238.
22 L. Mikac, A. Csáki, B. Zentai, I. Rigó, M. Veres, A. Tolić, M. Gotić and M. Ivanda, UV irradiation of polyethylene terephthalate and polypropylene and detection of formed microplastic particles down to 1 μm, *ChemPlusChem*, 2024, **89**(2), e202300497.
23 J. Ou, Y. Tang, E. A. Elimian, X. Yang, Y. Liu, Y. Fu, *et al.*, Transformation of microplastics during UV-LED based water disinfection: Mechanistic insights and environmental implications, *J. Hazard. Mater.*, 2025, 139121.
24 V. Hidalgo-Ruz, L. Gutow, R. C. Thompson and M. Thiel, Microplastics in the marine environment: a review of the methods used for identification and quantification, *Environ. Sci. Technol.*, 2012, **46**(6), 3060–3075.
25 A. Istomina, V. Chelomin, A. Mazur, A. Zhukovskaya, A. Karpenko and M. Mazur, Biodegradation of polyethylene in digestive gland homogenates of marine invertebrates, *PeerJ*, 2024, **12**, e17041.
26 K. Min, J. D. Cuiffi and R. T. Mathers, Ranking environmental degradation trends of plastic marine debris based on physical properties and molecular structure, *Nat. Commun.*, 2020, **11**(1), 727.
27 F. Sandro, H. Bodo and G. Detlef, Quantitative sizing of microplastics up to 20 μm using ICP-TOFMS, *J. Anal. At. Spectrom.*, 2025, **40**(1), 276–285.
28 P. O. Nyangaresi, T. Rathnayake and S. E. Beck, Evaluation of disinfection efficacy of single UV-C, and UV-A followed by UV-C LED irradiation on Escherichia coli, B. spizizenii and MS2 bacteriophage, in water, *Sci. Total Environ.*, 2023, **859**, 160256.
29 K. Mawatari, Y. Kadomura-Ishikawa, T. Emoto, Y. Onoda, K. Ishida, S. Toda, *et al.*, Viral Inactivation by Light-Emitting Diodes: Action Spectra Reveal Genomic Damage as the Primary Mechanism, *Viruses*, 2025, **17**(8), 1065.
30 A. C. Lorenzo-Leal, W. Tam, A. Kheyrandish, M. Mohseni and H. Bach, Antimicrobial activity of filtered far-UVC light (222 nm) against different pathogens, *BioMed Res. Int.*, 2023, **2023**(1), 2085140.
31 S. E. Beck, H. Ryu, L. A. Boczek, J. L. Cashdollar, K. M. Jeanis, J. S. Rosenblum, *et al.*, Evaluating UV-C LED disinfection performance and investigating potential dual-wavelength synergy, *Water Res.*, 2017, **109**, 207–216.
32 S. E. Beck, P. Suwan, T. Rathnayeke, T. M. H. Nguyen, V. A. Huanambal-Sovero, B. Boonyapalanant, *et al.*, Woven-fiber microfiltration (WFMF) and ultraviolet light emitting diodes (UV LEDs) for treating wastewater and septic tank effluent, *Water*, 2021, **13**(11), 1564.
33 S. Bounty, R. A. Rodriguez and K. G. Linden, Inactivation of adenovirus using low-dose UV/H2O2 advanced oxidation, *Water Res.*, 2012, **46**(19), 6273–6278.
34 J. A. MacDonald, B. Najm, T. Cath and W. A. Mitch, Purifying Anaerobically Treated Municipal Secondary Wastewater

Effluent by a Reverse Osmosis-Based Potable Reuse Treatment Train, *ACS ES&T Water*, 2025, 4877–4886.

35 Health Canada, *Guidelines for Canadian Drinking Water Quality: Guideline Technical Document- Escherichia coli*, Ottawa, Ontario: Water and Air Quality Bureau, Healthy Environments and Consumer Safety Branch, Health Canada, 2020, https://www.canada.ca/en/health-canada/services/publications/healthy-living/guidelines-canadian-drinking-water-quality-escherichia-coli.html.

36 M. Vasylius, A. Tadžijevas, D. Šapalas, V. Kartašovas, J. Janutėnienė and P. Mažeika, Degradation of mechanical properties of A-PET films after UV aging, *Polymers*, 2023, **15**(20), 4166.

37 E. Conterosito, M. Roncoli, C. Ivaldi, M. Ferretti, B. De Felice, M. Parolini, *et al.*, μ-FTIR Reflectance Spectroscopy Coupled with Multivariate Analysis: A Rapid and Robust Method for Identifying the Extent of Photodegradation on Microplastics, *Anal. Chem.*, 2025, **97**(6), 3263–3273.

38 M. Celik, H. Nakano, K. Uchida, A. Isobe and H. Arakawa, Comparative evaluation of the carbonyl index of microplastics around the Japan coast, *Mar. Pollut. Bull.*, 2023, **190**, 114818.

39 M. Zvekic, L. C. Richards, C. C. Tong and E. T. Krogh, Characterizing photochemical ageing processes of microplastic materials using multivariate analysis of infrared spectra, *Environ. Sci.: Processes Impacts*, 2022, **24**(1), 52–61.

40 S. Rostampour, R. Cook, S. S. Jhang, Y. Li, C. Fan and L. P. Sung, Changes in the chemical composition of polyethylene terephthalate under UV radiation in various environmental conditions, *Polymers*, 2024, **16**(16), 2249.

41 M. C. Lessa Belone, M. Kokko and E. Sarlin, Degradation of common polymers in sewage sludge purification process developed for microplastic analysis, *Environ. Pollut.*, 2021, **269**, 116235.

42 A. B. D. Nandiyanto, R. Ragadhita and M. Fiandini, Interpretation of Fourier transform infrared spectra (FTIR): A practical approach in the polymer/plastic thermal decomposition, *Indones. J. Sci. Technol*, 2023, **8**(1), 113–126.

43 S. Gomes R, A. N. Fernandes and W. R. Waldman, How to measure polymer degradation? An analysis of authors' choices when calculating the carbonyl index, *Environ. Sci. Technol.*, 2024, **58**(17), 7609–7616.

44 C. Campanale, I. Savino, C. Massarelli and V. F. Uricchio, Fourier transform infrared spectroscopy to assess the degree of alteration of artificially aged and environmentally weathered microplastics, *Polymers*, 2023, **15**(4), 911.

45 J. A. O. Brandão, F. D. P. Morisso, E. L. Francisquetti and R. M. C. Santana, FTIR as a tool to evaluate the photooxidative degradation of polyethylene, in *Congresso Brasileiro de Polímeros*, 2021 (16: 2021: online)[Anais] [recurso eletrônico] São Paulo: ABPol.

46 M. Brogly, S. Bistac and D. Bindel, Advanced surface FTIR spectroscopy analysis of poly (ethylene)-block-poly (ethylene oxide) thin film adsorbed on gold substrate, *Appl. Surf. Sci.*, 2022, **603**, 154428.

47 A. Gok, D. A. Gordon, D. M. Burns, S. P. Fowler, R. H. French and L. S. Bruckman, Reciprocity and spectral effects of the degradation of poly (ethylene-terephthalate) under accelerated weathering exposures, *J. Appl. Polym. Sci.*, 2019, **136**(22), 47589.

48 B. Du, C. Lee and Y. Ji, Study of Factors Affecting UV-Induced Photo-Degradation in Different Types of Polyethylene Sheets, *Polymers*, 2024, **16**(19), 2709.

49 F. J. Horne, J. J. Liggat, W. A. MacDonald and S. W. Sankey, Photo-oxidation of poly (ethylene terephthalate) films intended for photovoltaic backsheet, *J. Appl. Polym. Sci.*, 2020, **137**(17), 48623.

50 T. Sang, C. J. Wallis, G. Hill and G. J. P. Britovsek, Polyethylene terephthalate degradation under natural and accelerated weathering conditions, *Eur. Polym. J.*, 2020, **136**, 109873.

51 G. J. M. Fechine, P. A. Christensen, T. A. Egerton and J. R. White, Evaluation of poly(ethylene terephthalate) photostabilisation using FTIR spectrometry of evolved carbon dioxide, *Polym. Degrad. Stab.*, 2009, **94**(2), 234–239.

52 A. L. Andrady, *Plastics and the Environment*, John Wiley & Sons, 2003.

53 P. Pereira, P. E. Savage and C. W. Pester, Neutral hydrolysis of post-consumer polyethylene terephthalate waste in different phases, *ACS Sustain. Chem. Eng.*, 2023, **11**(18), 7203–7209.

54 C. V. Aarsen, A. Liguori, R. Mattsson, M. H. Sipponen and M. Hakkarainen, Designed to degrade: tailoring polyesters for circularity, *Chem. Rev.*, 2024, **124**(13), 8473–8515.

55 X. Liu and R. Yang, Conversion among photo-oxidative products of polypropylene in solid, liquid and gaseous states, *BMC Chem.*, 2020, **14**(1), 44.

56 S. S. Alavian Petroody, S. H. Hashemi, L. Škrlep, B. Mušič, C. A. van Gestel and A. Sever Škapin, UV light causes structural changes in microplastics exposed in bio-solids, *Polymers*, 2023, **15**(21), 4322.

57 V. P. Chelomin, A. A. Istomina, A. A. Mazur, V. V. Slobodskova, A. F. Zhukovskaya and N. V. Dovzhenko, New insights into the mechanisms of toxicity of aging microplastics, *Toxics*, 2024, **12**(10), 726.

58 G. Grause, M. F. Chien and C. Inoue, Changes during the weathering of polyolefins, *Polym. Degrad. Stab.*, 2020, **181**, 109364.

59 R. G. Zepp, B. Acrey, M. J. Davis, A. L. Andrady, J. Locklin, R. Arnold, *et al.*, Weathering effects on degradation of low-density polyethylene-nanosilica composite with added pro-oxidant, *J. Polym. Environ.*, 2023, **31**(10), 4184–4192.

60 M. H. Cho, Y. J. Song, C. J. Rhu and B. R. Go, Pyrolysis process of mixed microplastics using TG-FTIR and TED-GC-MS, *Polymers*, 2023, **15**(1), 241.

61 N. R. Maddela, D. Kakarla, K. Venkateswarlu and M. Megharaj, Additives of plastics: Entry into the environment and potential risks to human and ecological health, *J. Environ. Manage.*, 2023, **348**, 119364.

62 L. C. Matchett and S. A. Styler, Influence of microplastic colour on photodegradation of sorbed contaminants, *Environ. Sci.: Processes Impacts*, 2025, **27**(10), 3076–3082.

63 Y. Xu, Q. Ou, J. P. van der Hoek, G. Liu and K. M. Lompe, Photo-oxidation of micro-and nanoplastics: physical, chemical, and biological effects in environments, *Environ. Sci. Technol.*, 2024, **58**(2), 991–1009.
64 C. Maddison, C. I. Sathish, D. Lakshmi, O. Wayne and T. Palanisami, An advanced analytical approach to assess the long-term degradation of microplastics in the marine environment, *npj Mater. Degrad.*, 2023, **7**(1), 59.
65 K. Brožová, S. Heviánková, J. Halfar, K. Čabanová and A. Valigůrová, Plastic degradation in aquatic environments: a review of challenges and the need for standardized experimental approaches, *Front. Environ. Sci.*, 2025, **13**, 1677793.